

T₁ mapping of the mouse brain following fractionated manganese administration using MP2RAGE

Luc Driencourt¹ · Carola Jacqueline Romero¹ · Mario Lepore¹ · Florent Eggenschwiler¹ · Olivier Reynaud¹ · Nathalie Just^{1,2}

Received: 26 November 2015 / Accepted: 3 March 2016 / Published online: 21 March 2016
© Springer-Verlag Berlin Heidelberg 2016

Abstract With the increasing development of transgenic mouse models of neurodegenerative diseases allowing improved understanding of the underlying mechanisms of these disorders, robust quantitative mapping techniques are also needed in rodents. MP2RAGE has shown great potential for structural imaging in humans at high fields. In the present work, MP2RAGE was successfully implemented at 9.4T and 14.1T. Following fractionated injections of MnCl₂, MP2RAGE images were acquired allowing simultaneous depiction and T₁ mapping of structures in the mouse brain at both fields. In addition, T₁ maps demonstrated significant T₁ shortenings in different structures of the mouse brain ($p < 0.0008$ at 9.4T, $p < 0.000001$ at 14.1T). T₁ values recovered to the levels of saline-injected animals 1 month after the last injection except in the pituitary gland. We believe that MP2RAGE represents an important prospective translational tool for further structural MRI.

Keywords T₁ relaxation · Mouse · MEMRI · High resolution · Translational

Electronic supplementary material The online version of this article (doi:10.1007/s00429-016-1211-3) contains supplementary material, which is available to authorized users.

✉ Nathalie Just
nathalie.just@ukmuenster.de

¹ CIBM-AIT Core, Ecole Polytechnique Fédérale de Lausanne, Lausanne, Switzerland

² Institut für Klinische Radiologie, Translational Research Imaging Center (TRIC), Albert-Schweitzer-Campus 1, Gebäude A16, Anfahrt: Waldeyerstr. 1, 48149 Münster, Germany

Abbreviations

MP2RAGE	Magnetization-prepared 2 rapid acquisition gradient echo sequence
MEMRI	Manganese-enhanced MRI
FLASH	Fast-low angle shot
SNR	Signal-to noise-ratio
CNR	Contrast-to-noise ratio
GRE	Gradient echo
FASTMAP	Fast, automatic shimming technique by mapping along projections

Introduction

In 2010, Marques et al. (2010) proposed the Magnetization-Prepared 2 Rapid acquisition Gradient echo sequence (MP2RAGE) allowing rapid 3D bias field free acquisition of T₁-weighted images at an increased spatial resolution. The technique not only permits the fast elimination of spatial inhomogeneities inherent to high fields but also enables simple calculation of accurate T₁ maps using look-up tables. To date, MP2RAGE remains a clinical MR sequence allowing high spatial resolution (<1 mm³ in 10 min), robust T₁ structural brain imaging (O'Brien et al. 2014) and lesion assessment (Kober et al. 2012) due to the high grey-to-white matter contrast offered by the human brain at high field.

With the availability of transgenic mice models of neurological disorders, investigation of small structures in the mouse brain using T₁-based techniques has gained more and more interest (van de Ven et al. 2007). At higher fields (≥9.4T), although susceptibility effects are increased, gains in SNR and T₁ spin lattice relaxation times (van de Ven et al. 2007) allow investigation of wider

ranges of T_1 values as well as detection of specific tissue features such as myelin (Labadie et al. 2014).

Improved visualization of brain neuro-architecture was obtained using high-resolution T_1 -weighted techniques such as manganese-enhanced MRI (MEMRI) at higher field strengths. MEMRI represents nowadays a key molecular MR imaging technique where the paramagnetic properties of Mn^{2+} allow indirect access to neuronal activation (Auffret et al. 2016) and anterograde neuronal tract tracing (Canals et al. 2008). Accumulation of Mn^{2+} in brain structures provides increased signal-to-noise ratios (SNR) and contrast-to-noise ratios (CNR) and depends on various factors such as neuronal density, function, dose and metal transporters that remain poorly understood. To date one of the major limiting factors in MEMRI studies is the toxicity of manganese at high doses [>45 mg/kg (Silva et al. 2004)] and the poor sensitivity of MRI techniques at low doses.

In this study, we aimed at implementing the MP2RAGE sequence at 9.4T and 14.1T for an improved T_1 quantitative mapping of the mouse brain architecture. In order to compensate for the lack of contrast between grey and white matter in the mouse brain, systemic fractionated manganese injections were performed allowing quantitative investigations of manganese-enhanced structures up to 1 month after the last injection with little toxicity. The translational value of MP2RAGE in small rodents was further investigated with an emphasis on CNR.

Materials and methods

Theory

The MP2RAGE sequence starts with a 180° adiabatic inversion pulse followed by a first gradient echo block within which a low flip angle α_1 is repeated nPE_1 times with a repetition time TR. A second gradient echo block is acquired with a low flip angle α_2 . Two images with k-space centres corresponding to T_{11} and T_{12} , respectively, are acquired. The sequence is repeated nPE_2 times to encode the third dimension. The time between two 180° adiabatic pulses is T . Hence, two 3D MR images are obtained (Fig. 1). These images can be combined as described in Marques et al. (2010) using Eq. (1):

$$S = \text{real} \left(\frac{GRE_{T_{11}}^* GRE_{T_{12}}}{|GRE_{T_{11}}|^2 + |GRE_{T_{12}}|^2} \right), \quad (1)$$

where S represents the MP2RAGE signal, $GRE_{T_{11}}$ represents the signal acquired for each image of the first gradient echo block after an inversion time T_{11} and $GRE_{T_{11}}^*$ stands for its complex conjugate. $GRE_{T_{12}}$ represents the signal acquired for each image of the second gradient echo block after an inversion time T_{12} .

There are several advantages to combining images with Eq. (1): removal of signal dependence on M_0 , T_2^* and reception sensitivity can be demonstrated by derivation of the signal expression of Eq. (1) (see Appendix 1 in Mar-

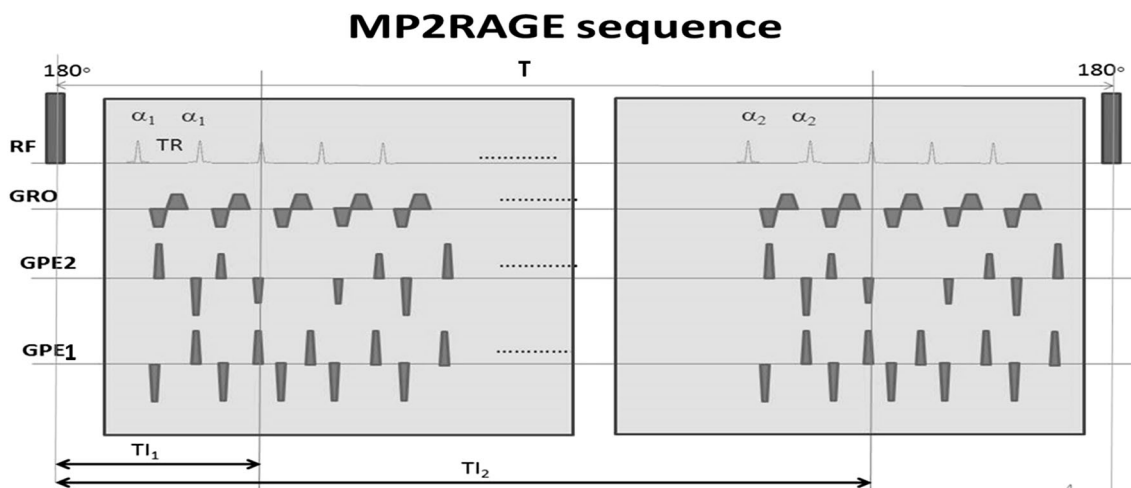


Fig. 1 Diagram of the MP2RAGE sequence. T_{11} and T_{12} represent the respective inversion time delays from the *middle* of the adiabatic inversion 180° pulse to the excitation pulse (α_1 and α_2 , respectively) at the *centre* of the k-space line. T is the repetition time between two successive inversion pulses. TR is the repetition time between successive gradient echo excitation pulses in each block. Two images with k-space centres corresponding to T_{11} and T_{12} , respectively, are

acquired. The sequence is repeated nPE_2 times to encode the third-dimension. *RF* radio frequency pulses, *GRO* readout gradient, *GPE₁* phase encode gradient, *GPE₂* second phase encode gradient for encoding of the third gradient. Replacing the 180° adiabatic inversion pulse by a 90° saturation pulse as well as the inversion times T_{11} and T_{12} by TS_1 and TS_2 , respectively, the SA2RAGE sequence for B_1 mapping can be obtained

ques et al. 2010) while the dynamic range of signal intensities is constrained between -0.5 and 0.5 . The contrast-to-noise ratio (CNR) of the combined image can be conserved (or enhanced) although the signal-to-noise ratio may be reduced due to noise propagation (Marques et al. 2010). CNR per unit time was simulated for various combinations of T , T_{11} , T_{12} , α_1 and α_2 parameters (Marques et al. 2010) at 3T and 7T using Eq. (2):

$$\text{CNR}_{1,2} = \frac{S_1 - S_2}{\sqrt{\sigma_1^2 + \sigma_2^2}} \times \frac{1}{\sqrt{\text{MP2RAGETR}}}, \quad (2)$$

where S_1 and S_2 represent the respective MP2RAGE signals for tissue 1 and tissue 2. σ_1 and σ_2 represent the noise of the MP2RAGE signal for tissue 1 and tissue 2 respectively and were calculated via error propagation of Eq. 1.

Essentially, apart from the field dependence of WM and GM T_1 values, these simulations remain valid for our study.

In the present work, we investigated the optimization of MP2RAGE parameters with regard to assumed literature T_1 values of the mouse brain from reference (Chuang and Koretsky 2006; Lee et al. 2005). Thus, T_1 values were chosen as 1.2/1.8/2.5 s in white, grey matter and cerebrospinal fluid (WM, GM, CSF), respectively, assuming that these values measured at 11.7T in mice represent a good compromise for optimizing contrast-to-noise ratio in the mouse brain at 9.4T and 14.1T. However, without contrast agent to enhance visualization of architecture on T_1 -weighted MR images, the normal mouse brain is poorly contrasted (Chuang and Koretsky 2006). We used fractionated injections of MnCl_2 to investigate T_1 differences between tissues. Based on T_1 values measured in references (Chuang and Koretsky 2006; Lee et al. 2005) and previous in-house pilot studies, T_1 values upon 30 mg/kg MnCl_2 injections were chosen as 0.5/0.8/2.8 s (WM, GM, CSF) assuming again a good compromise between 9.4T and 14.1T fields and displaying optimized CNR values for $\text{MP2RAGETR}/T_{11}/T_{12}/\alpha_1/\alpha_2 = 4\text{--}8.25$ s/0.6–1 s/2.0–3.5 s/4–7°/4–7° according to simulations presented in Marques et al. (2010). T_1 mapping was obtained using look-up tables derived from Bloch simulations of the MP2RAGE sequence (Marques et al. 2010) and the optimized parameters defined earlier together with the inversion efficiency of the adiabatic inversion pulse set at 0.9 and the number of phase encoding steps. The T_1 value of each pixel was obtained via linear interpolation (Marques et al. 2010).

B₁ mapping

The combined MP2RAGE image remains dependent on the transmit B_1 field (see Appendix 1 in Marques et al. 2010). In order to evaluate the transmit B_1 field (B_1^+), the

SA2RAGE sequence was used. This sequence was described by Eggenschwiler et al. (2012) and can be defined in an identical way to the MP2RAGE sequence albite starting with a 90° saturation pulse instead of the adiabatic inversion pulse of the MP2RAGE. Parameters were chosen as described by Eggenschwiler et al. (2012) using $T/T_{11}/T_{12}/\alpha_1/\alpha_2 = 2.4$ s/100/1800 ms/4°/11°. As for T_1 evaluation, Bloch simulations of the SA2RAGE signal were performed using the parameters defined earlier. Look-up tables linking B_1 to SA2RAGE ratio were obtained allowing B_1 estimates on a pixel by pixel basis by linear interpolation.

Phantom

To validate the MP2RAGE T_1 measurements, a phantom consisting of a 26G-syringe filled with demineralized water and 10 MnCl_2 -doped NMR tubes (0–500 μM) was imaged using in-house-made volume coils at 9.4T and 14.1T (Cheng et al. 2014) using an inversion-recovery fast spin echo sequence (IR-FSEMS: TR = 15000 ms; 20 TIs = 100–1800 ms; (Echo Spacing (ESP) = 8.30 ms; Echo-train Length (ETL) = 8; FOV = 40 × 40 mm²; Matrix = 128 × 128; four slices; Thickness (THK) = 2 mm; Acqtime = 2 h) after manual shimming. MP2RAGE images were acquired with the following parameters: MP2RAGE TR = 4000 ms; $\text{TR}_{\text{GRE}}/\text{TE} = 10/2.1$ ms; FOV = 40 × 40 × 40 mm³; Matrix = 128 × 128 × 32; $T_{11} = 320$ ms; $T_{12} = 2280$ ms; flip angle1 = 2, 4, 7, 10°; flipangle2 = 2, 3, 4, 5, 7, 11 or 15°. Two stacks of 256 images were obtained in 4 min 16 s. Images were reconstructed offline and analysed with in-house written Matlab routines (The Mathworks, USA). T_1 values obtained with IR-FSEMs and MP2RAGE were correlated.

Animals

Animal preparation

All animal experiments were approved by the Veterinary Office of Canton de Vaud and conducted according to the federal and local ethical guidelines, EXPANIM (Expérience sur animaux- SCAV, Service de la consommation et des affaires vétérinaires, Switzerland). Experiments were carried out using 30 adult C57BL6 mice weighing 30–35 g (15 at 9.4T and 15 at 14.1T). An isotonic solution of MnCl_2 (Sigma, Aldrich, St. Louis, MO) was prepared at a concentration of 15 mM MnCl_2 and injected into awake mice through an intraperitoneal (IP) MnCl_2 injection. Control mice received IP injections of normal saline solution. MnCl_2 was administered using a fractionated scheme of injection (Grünecker et al. 2010) to minimize toxicity effects. 20 mice received a 30 mg/kg MnCl_2 and 10 mice

received an equivalent volume of saline (NaCl 0.9 %) at 17 h for five consecutive days (5×30 mg/kg/24 h). Each mouse was weighed and temperature-controlled after each injection and subsequently on each scanning day. After MnCl_2 injections, the animals were returned to their cages and allowed free access to food and water.

Prior to imaging, each animal was anaesthetized (2–3 % Isoflurane in air) and set into an MR-compatible cradle. During MRI, the animals were anaesthetized by breathing 1 % isoflurane into oxygen-enriched air with a facemask. The rectal temperature was carefully monitored and maintained at 36 ± 1 °C. Their respiration rate was monitored with a pressure captor placed underneath the mouse body and was maintained above 80 breaths/min. MEMRI was performed 20–24 h after the last MnCl_2 administration for all T_1 measurements. Three animals per session were scanned. One of these animals was a saline-injected animal. The same animals were re-scanned at 48, 96 h, 1 week and 1 month after the last IP MnCl_2 injection.

Manganese-enhanced MRI

All MRI experiments were performed either on a 9.4T/31 cm horizontal bore magnet (Varian, Agilent, USA) or on a 14.1T/26 cm (Varian, Agilent, USA) one. The magnets were equipped with 12-cm inner-diameter actively shielded gradient sets (Magnex Scientific, Oxford, UK) allowing a maximum gradient of 400 mT/m in 120 μs . Home-built quadrature T/R 14-mm surface coils were used. Field homogeneities were adjusted using an EPI version of FASTMAP (Tkáč et al. 2004). After the preliminary adjustments (tuning, shimming, acquisition of scout images for accurate positioning) fast spin echo (FSEMS) images (TR/TE = 2500/12 ms, 8 echoes, FOV = 25×25 mm, matrix size = 256×256 ; axial slices, TH = 0.5 mm, eight averages) were acquired. 3D gradient echo T_1 -weighted images (TR/TE = 25/3 ms, Flip angle = 70° , FOV = $20 \times 20 \times 25$ mm³, matrix size = $128 \times 128 \times 128$, coronal slices, BW = 25 kHz, three averages) were acquired as part of the MEMRI protocol. MP2RAGE images were obtained after shimming with FASTMAP over a centred voxel covering the mouse brain $8 \times 8 \times 8$ mm³. The choice of flip angles was based on the combination of flip angles giving the best agreement between T_1 s measured with IR-FSEMS and MP2RAGE techniques in phantoms.

Image analysis and statistics

MR images were processed and analysed using Image processing software (Image J 1.3.1_13, NIH, USA) as well as custom-written routines running in MATLAB (MATLAB 14, The MathWorks, USA).

The CNR of MP2RAGE combination of images was calculated using Eq. (2). For in vivo experiments, CNR was evaluated by manually drawing regions of interest (ROI) of identical sizes in WM and GM structures of the cerebellum and in the colliculus and CA3 structures. SNR of the MP2RAGE combination of images was calculated as the ratio of the signal calculated with Eq. (1) to the noise propagation characteristics and according to equations defined in (Marques et al. 2010).

For all other images, SNR was calculated as the ratio of the signal to the standard deviation of the noise in regions of interest (ROI) drawn in the cortex, cerebellum, ventricles, thalamus, caudate putamen (CPu), hypothalamus, pituitary gland and hippocampus. The average SNR across all ROIs was also calculated. ROIs were defined bilaterally on 3D- Gradient Echo T_1 -weighted images and relative to the Paxinos and Watson's atlas (1998) and transferred to the T_1 maps to ensure precise positioning. In order to avoid overestimation of noise levels using ROIs, noise levels were estimated from the Rician distribution of magnitude images using the methodology proposed in Rajan et al. (2010). Estimates of SNR and CNR using the two methods were compared. T_1 maps were generated for an entire 3D volume acquired for each animal. Mean T_1 values were calculated from the ROIs drawn on T_1 maps. Mean T_1 values were compared with a one-way ANOVA corrected for Bonferroni test. Body weights and temperatures during the fractionated injection procedure and follow-up were compared using an unpaired *t* test. A *p* value < 0.05 was considered significant. Data are represented as mean \pm mean standard error (SEM) unless otherwise stated.

Results

Optimization of MP2RAGE for imaging mice

During the fractionated injection protocol, no significant difference was found in terms of body weight between saline-injected and Mn^{2+} -injected animals (*t* test, *p* > 0.05) (Fig. S1A). Moreover, no significant difference was found between the temperature of saline-injected and MnCl_2 -injected mice either during the fractionated injection procedure or after cessation of Mn^{2+} injections although the average temperature difference was -0.2 ± 0.1 °C between the two groups (Fig. S1B). There was no significant influence of time either (*t* test, *p* > 0.05).

Figure 2 shows examples of magnitude and phase images at two inversion times, their combination using Eq. (1) and their corresponding T_1 maps using look-up tables. Images at 9.4T and 14.1T with differing spatial resolutions are presented. Phase images show important distortions at both field strengths due to remaining macroscopic B_0

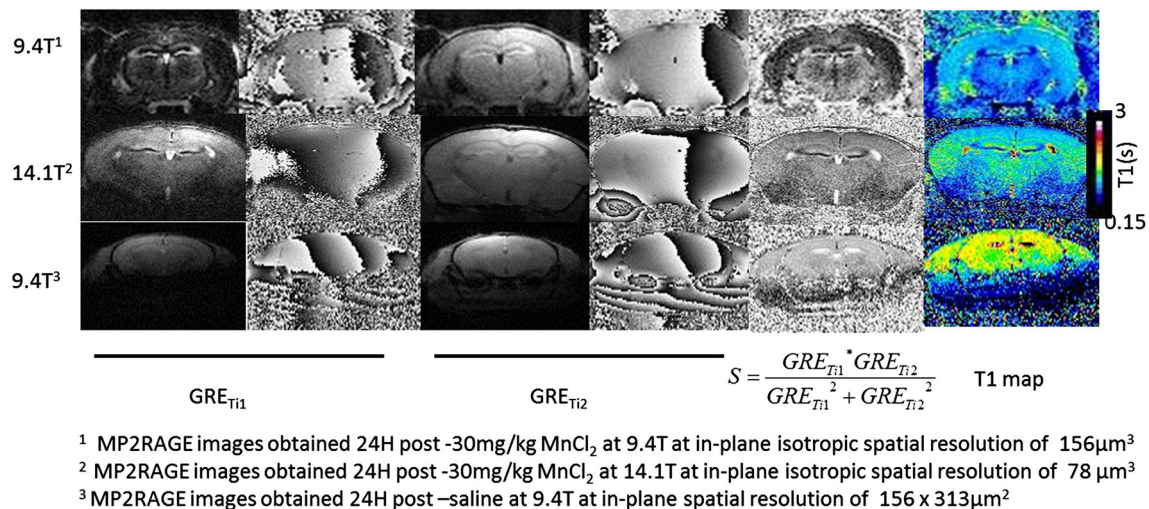


Fig. 2 Representative coronal slices obtained with the MP2RAGE sequence at 9.4T and 14.1T and different spatial resolutions. Magnitude and phase images at both inversion times (T_{11} and T_{12})

are shown as well as their combinations [in the $(-0.5, 0.5)$ signal intensity (S) range] and the resulting T_1 maps

regional variations despite second-order FASTMAP shimming over a large cubic area. Nonetheless, the image combination resulted in images with good contrast and bias field cancellation at both fields allowing computation of T_1 maps at different spatial resolutions.

The influence of acquisition parameters such as T , flip angles and inversion times was further investigated for optimization purposes. In Fig. 3a, the signal for each of the gradient echo images was simulated for different parameters, subsequently allowing to numerically simulate MP2RAGE signal as a function of T_1 for different sets of parameters (Fig. 3b) without noise contamination. These look-up tables (LUT) can subsequently be used to estimate T_1 values on a pixel-by-pixel basis. LUT show that the range of T_1 values (500–3000 ms) that we expected to cover after MnCl₂ injection was reached for the chosen inversion times (T_{11}/T_{12}) and flip angles. T_1 estimates above 3000 ms (for flip angles 2/2° and 4/4°) and above 2500 ms (for flip angles 7/7°) became less reliable. In addition, the contrast-to-noise ratio (CNR) per unit time was estimated for different combinations of parameters (Fig. 3c). Numerical simulations demonstrated that CNR was increased as T and flip angles were increased while the range of chosen T_1 values was strongly linked to the flip angles for high CNR. For flip angles (2, 2°) and (4, 4°) and $T_{11,2} = 800$ –1600 ms, the CNR per unit time was between 3 and 6.25 times lower than for flip angles (7, 7°). Coronal MP2RAGE images of mice 24 h after 5×30 mg/kg MnCl₂ IP injection are shown in Fig. 3d–f and were acquired at 9.4T with the parameters used for simulations. Images with flip angles (2, 2°) and (7, 7°) were acquired in the same animal and images with flip angles (4, 4°) in another mouse. The comparison of the MP2RAGE combination of images allowed evaluating the impact of noise. Visually and qualitatively, a

higher CNR can be appreciated on Fig. 3f where a clearer delineation of WM/GM structures in the cerebellum can be noticed compared to Fig. 3d. This was confirmed quantitatively where a fourfold increase in CNR between WM/GM in the cerebellum was obtained while the contrast colliculus/CA3 was increased 25-fold for MP2RAGE combination of images acquired with flip angles (7, 7°) and $T_{11,2} = 800/1600$ ms due to improved SNR levels and less partial volume effects. There was little difference between CNR estimates for MP2RAGE combinations of images with flip angles (2, 2°) and (4, 4°). Further discrepancies in in vivo data can be explained by the transmit field B_1 distortions that affect first and second contrasts differently. B_1 mapping was performed using the SA2RAGE sequence (Eggenschwiler et al. 2012) as shown in Fig. 4, which is representative of the field maps obtained with transmit/receive quadrature surface coils at 9.4T and 14.1T. B_1 values can be linked to the ratio of images obtained at two saturation times by solving Bloch equations and constructing a look-up table (Fig. 4a). This LUT was used for mapping B_1 on a pixel by pixel basis (Fig. 4b). Longitudinal and transversal B_1 profiles (Fig. 4c, d respectively) showed a variation of 50 % in B_1 from top (near the surface coil) to bottom of the mouse brain and 30 % from right to left.

In order to correct for transmit field inhomogeneity, the accuracy of pulse profiles was investigated. T_1 -weighted MP2RAGE images were acquired at 9.4T and 14.1T with $T_{11} = 320$ ms and $T_{12} = 2280$ ms to cover the range of T_1 values of the ten different MnCl₂-doped vials (Fig. 4e). T_1 values acquired with MP2RAGE in the phantom for various combinations of flip angles were correlated to T_1 s measured with IRFSEMS. T_1 values were the most accurate for flip angles 2, 2° and 2, 3° at 9.4T and 14.1T, respectively. However, these low flip angle values

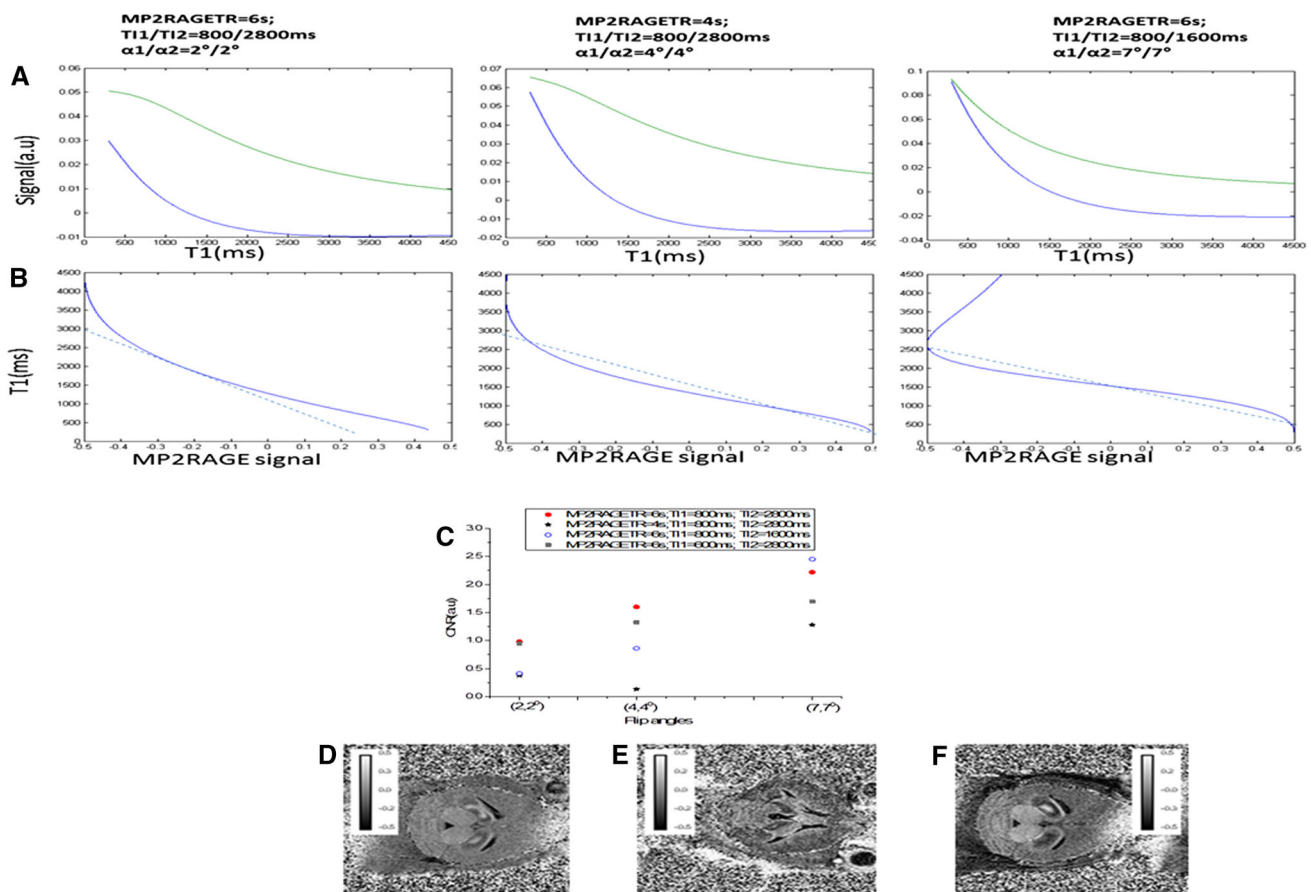


Fig. 3 Optimization of MP2RAGE $T_{11,2}$, T and α_1/α_2 parameters. **a** First gradient echo signals (blue) and 2nd gradient echo signals (green) of the MP2RAGE sequence as a function of T_1 were simulated using Bloch equations (Marques et al. 2010, Appendix1) and different sets of parameters. **b** The preceding simulated signals were combined using Eq. (1) allowing an evaluation of the MP2RAGE signal as a function of T_1 . Each look-up table was obtained using the different sets of parameters. Dashed lines were added to indicate the linear part of the T_1 -MP2RAGE signal relationship. **c** The contrast-to-noise ratio (CNR) was simulated using Eq. (2) and the three different sets of parameters already used. An extra set of parameters: $T/T_{11}/T_{12} = 6000/600/2800$ ms and $\alpha_1 = 2, 4, 7^\circ$ and $\alpha_2 = 2, 4, 7$ was also simulated. **d-f** In vivo data at 9.4T:

corresponded to an important drop in CNR as showed by CNR evaluations in Fig. 3d. In the present study, we privileged accurate T_1 estimates versus higher CNR and we used these values for further measurements in mice.

MEMRI of mouse brain with MP2RAGE

Figure 5 shows coronal slices at the same position from a T_1 -weighted gradient echo 3D MRI (Fig. 5a), the first block of 3D MR gradient echo images of MP2RAGE ($T/TR/TE$ (ms)/ $\alpha_1 = 6000/10/4/2^\circ$; BW = 50 kHz; FOV = $20 \times 20 \times 25$ mm³; Matrix = 128^3 ; $T_{i1} = 800$ ms; Fig. 5b) and the second block of 3D MR gradient echo images of MP2RAGE ($T_{i2} = 2800$ ms/ $\alpha_2 = 2^\circ$; Fig. 5c) of a mouse brain acquired

horizontal planes showing MP2RAGE combinations of images (-0.5 – 0.5 signal range) for each set of parameters. Images with $\alpha_1/\alpha_2 = 2, 2^\circ$ and $\alpha_1/\alpha_2 = 7, 7^\circ$ were acquired in the same animal. $CNR_{Colliculus/CA3} = 9\%$ vs $CNR_{Colliculus/CA3} = 222\%$; $CNR_{GM/WM} = 31.4\%$ vs $CNR_{GM/WM} = 134\%$ in the cerebellum for respective flip angle pairs. $CNR_{Colliculus/CA3} = 14\%$ for $\alpha_1/\alpha_2 = 4, 4^\circ$. (In addition, CNR was calculated for each magnitude image S_1 and S_2 (Eq. 1) using the image noise evaluated with the Rician distribution such that $CNR_{Colliculus/CA3} = 0.99/2.43$ vs $CNR_{Colliculus/CA3} = 1.88/3.54$; $CNR_{GM/WM} = 0.220/1.45$ vs $CNR_{GM/WM} = 1.74/1.11$ in the cerebellum for respective flip angle pairs. $CNR_{Colliculus/CA3} = 0.09/0.50$ for $\alpha_1/\alpha_2 = 4, 4^\circ$)

24 h after the last IP 30 mg/kg MnCl₂ fractionated injection (5×30 mg/kg/24 h) at 9.4T. Compared to 3D GRE MR images, the SNR of MP2RAGE images (1st block) was lower ($SNR_{average} = 15 \pm 6$ vs 9 ± 3). As expected, with our choice of parameters, the second block of MP2RAGE images was more proton-density weighted showing less contrast. Images acquired with the first and the second blocks were combined using Eq. (1) yielding MP2RAGE images (Fig. 5d) and T_1 maps (Fig. 5e). Although, the sensitivity of the surface coil decreased as a function of depth and the first and second blocks of GRE images were strongly affected by bias field effects and a decreased SNR compared to conventional 3D GRE, the MP2RAGE combination of images were cleared from reception field distortions and T_2^* effects. In MP2RAGE coronal

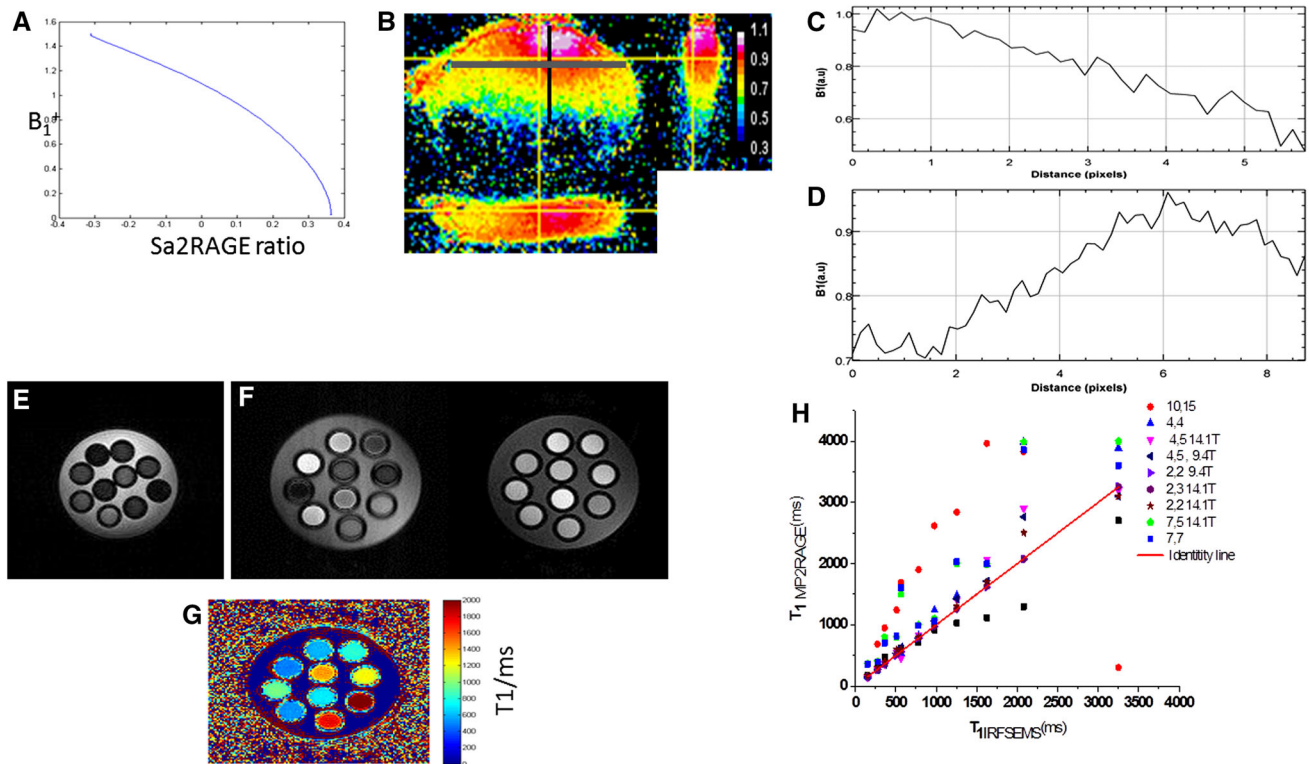


Fig. 4 B_1 mapping using the SA2RAGE sequence. **a** B_1 as a function of the SA2RAGE ratio obtained from Bloch simulations of the SA2RAGE signals (Eggenschwiler et al. 2012). **b** This look-up table was used to map the B_1^+ field on a pixel-by-pixel basis in the rat brain in the *three* directions. The *black vertical* and *grey horizontal* profiles served for evaluating **c** the B_1 *vertical* profile and **d** the B_1 *horizontal* profile as a function of distance in the rat brain showing that the sister sequence of MP2RAGE is useful for B_1 mapping and that important B_1 fluctuations were generated using our quadrature surface coils. **e** A phantom consisting of a 26G-syringe filled with demineralized water and 10 MnCl_2 doped NMR tubes (0–500 μM) was imaged using in-house made volume coils at 9.4T and 14.1T (Cheng et al. 2014) using an inversion-recovery fast spin echo

sequence (IRFSEMS) ($\text{TR} = 15000$ ms; $20 T_1s = 100$ – 1800 ms; $\text{ESP} = 8.30$ ms; $\text{ETL} = 8$; $\text{FOV} = 40 \times 40 \text{ mm}^2$; $\text{Matrix} = 128 \times 128$; four slices; $\text{THK} = 2$ mm; $\text{Acqtime} = 2$ h) after manual shimming. **f** 3D MP2RAGE images were then acquired with the following parameters: $T_{\text{MP2RAGE}} = 4000$ ms; $\text{TR}_{\text{GRE}}/\text{TE} = 10/2.1$ ms; $\text{FOV} = 40 \times 40 \times 40 \text{ mm}^3$; $\text{Matrix} = 128 \times 128 \times 32$; $T_{11} = 320$ ms; $T_{12} = 2280$ ms; flip angle one = 2° , 4° , 7° , 10° ; flip angle two = 2, 3, 4, 5, 11 or 15° . 3D stacks of 256 images were obtained in 4 min 16 s. **g** T_1 map for flip angles (2° , 3°) at 14.1T. **h** T_1 values acquired with MP2RAGE in the phantom for various combinations of flip angles were correlated to T_1 s measured with IRFSEMS. The best combination of flip angles was 2, 2° and 2, 3° , respectively, at 9.4T and 14.1T

views, the hippocampus showed clear delineation of CA1, CA2 and CA3 fields as well as dentate gyrus (DG) as seen in the false colour-coded inset. Strong uptake of Mn^{2+} could also be seen in the globus pallidus (GP, blue arrows). An enhanced contrast to noise ratio compared to T_1 -weighted GRE images (1st block) allowed delineation of the thalamus and hypothalamus as well as visualization of cortical layers (Fig. S2) and layers of the olfactory bulb (OB). Corresponding T_1 maps were constructed using the LUT related to the acquisition parameter used (Fig. 3b).

T_1 mapping with MP2RAGE at 9.4T and 14.1T at 24 h post- Mn^{2+} injection

Examples of T_1 coronal maps of the mouse brain acquired 24 h after the last MnCl_2 IP injection in saline-injected

mice (Fig. 6a) and in 5x30 mg/kg/24 h-injected mice at 9.4T and 14.1T respectively (Fig. 6b, c) are shown with little susceptibility artefacts and no bias field effects. There was a good contrast at 9.4T and 14.1T between CSF, cortical, thalamic and hypothalamic tissues. At the same dose of MnCl_2 (24 h post- 5×30 mg/kg), direct visualization of the increased T_1 length at 14.1T compared to 9.4T could be observed and were corroborated quantitatively in several structures of the mouse brain (Fig. 6d). At 9.4T the average brain T_1 across five mice was 1460 ± 220 and 1771 ± 121 ms at 14.1T in saline injected animals ($p < 0.004$, ANOVA). At 24 h post 5×30 mg/kg injection, average brain T_1 across ten mice was 1041 ± 330 ms at 9.4T and 1303 ± 486 ms at 14.1T representing a mean increase of 21 to 25 % respectively of T_1 values at 14.1T. However, T_1 values in individual structures were not significantly higher at 14.1T than at 9.4T after fractionated

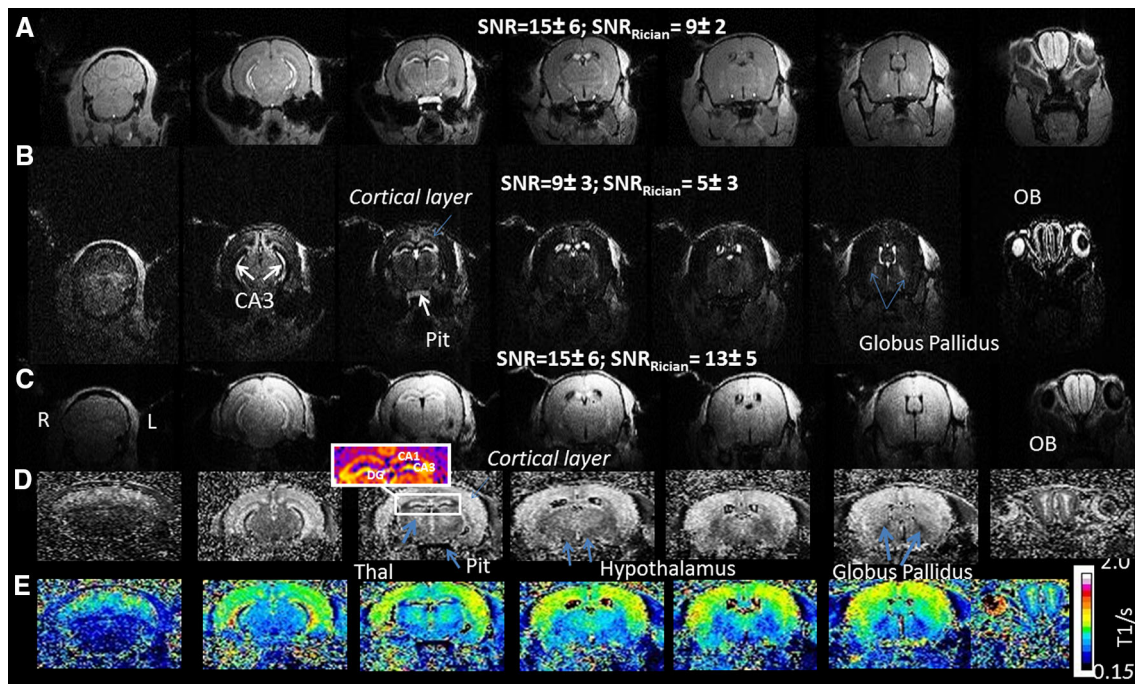


Fig. 5 **a** Coronal slices from a T_1 -weighted gradient echo 3D MRI [first row, TR/TE (ms)/ $\alpha = 25/4/45^\circ$; BW = 23 kHz; FOV = $20 \times 20 \times 25$ mm³; Matrix = 128^3 ; 9.4T]. **b** the first block of 3D MR gradient echo images of MP2RAGE [T/TR/TE(ms)/ $\alpha_1 = 6000/10/4/2^\circ$; BW = 50 kHz; FOV = $20 \times 20 \times 25$ mm³; Matrix = 128^3 ; $T_{i1} = 800$ ms] at the same position. **c** The second block of 3D MR gradient echo proton-density-weighted images of MP2RAGE ($T_{i2} = 2800$ ms/ $\alpha_2 = 2^\circ$) of a mouse brain acquired 24 h after the last IP 30 mg/kg $MnCl_2$ fractionated injection (5×30 mg/kg/24H) at 9.4T. These images were strongly affected by bias field

effects (Right side, R). Average SNR values are indicated for each series of images. **d** Corresponding combination of MP2RAGE images according to Eq. (1). The hippocampus was enlarged and colour-coded as shown in the inset for a better visualization of CA1, CA3 and DG. Using Eq. (1), bias field effects from the receive field were eliminated. **e** Corresponding T_1 maps for each coronal slice obtained on a pixel-by-pixel basis using a look-up table (Fig. 3b). T_1 values were estimated via linear interpolation. CA1, CA3: formation of the hippocampus, DG dentate gyrus, Thal thalamus, Pit pituitary gland, OB olfactory bulb

manganese injections (Fig. S3). T_1 s in Mn^{2+} -enhanced regions dropped significantly in most of the structures relative to T_1 s in saline-injected mice ($p < 0.01$ at 9.4T; $p < 0.008$ at 14.1T; Fig. 6e). Due to the presence of Mn^{2+} , the most important T_1 shortening was obtained in the pituitary gland [-60% ($p < 0.0008$) and -64% ($p < 0.000001$) at 9.4T and 14.1T respectively].

Evaluation of T_1 values during $MnCl_2$ elimination

T_1 values measured 24 h post-cessation of manganese injections in several brain structures at 14.1T, were significantly different from T_1 values measured in saline-injected animals ($p < 0.0008$) (Fig. 7a). 72 h post-cessation of manganese T_1 values remained significantly different in the cerebellum, the thalamus and the pituitary gland compared to T_1 values in saline-injected animals. 96 h post-cessation of manganese, only T_1 in the pituitary gland was significantly lower than in saline-injected animals ($p < 0.001$). Within 1 week after cessation of manganese injections, cortical and ventricular T_1 values measured at 9.4T had returned to the level of T_1 values measured in

saline-injected mice ($p > 0.05$) while cerebellum, CPu, hypothalamus, hippocampus and pituitary gland T_{1s} remained significantly lower ($p < 0.05$) than in saline-injected animals. After 1 month, T_1 values had recovered to the levels of saline-injected mice in almost all the structures except for the hypothalamus ($p < 0.05$) the pituitary gland ($p < 0.02$). On average, after cessation of Mn^{2+} injections, T_1 values had increased by more than 33 % after 1 week and 60 % after 1 month in almost all the structures. Interestingly, the pituitary gland T_1 only recovered 30 % of its initial value after 1 month (Fig. 7c).

Discussion

In the present study, the MP2RAGE sequence was used for the first time in mice at 9.4T and 14.1T. Whilst the mouse brain has inherently less contrast than the human brain, we used Mn^{2+} , known to enhance delineation of neuro-architecture, in order to demonstrate the translational value of the MP2RAGE technique. Mice models are particularly suited for MRI investigations at higher field strengths as

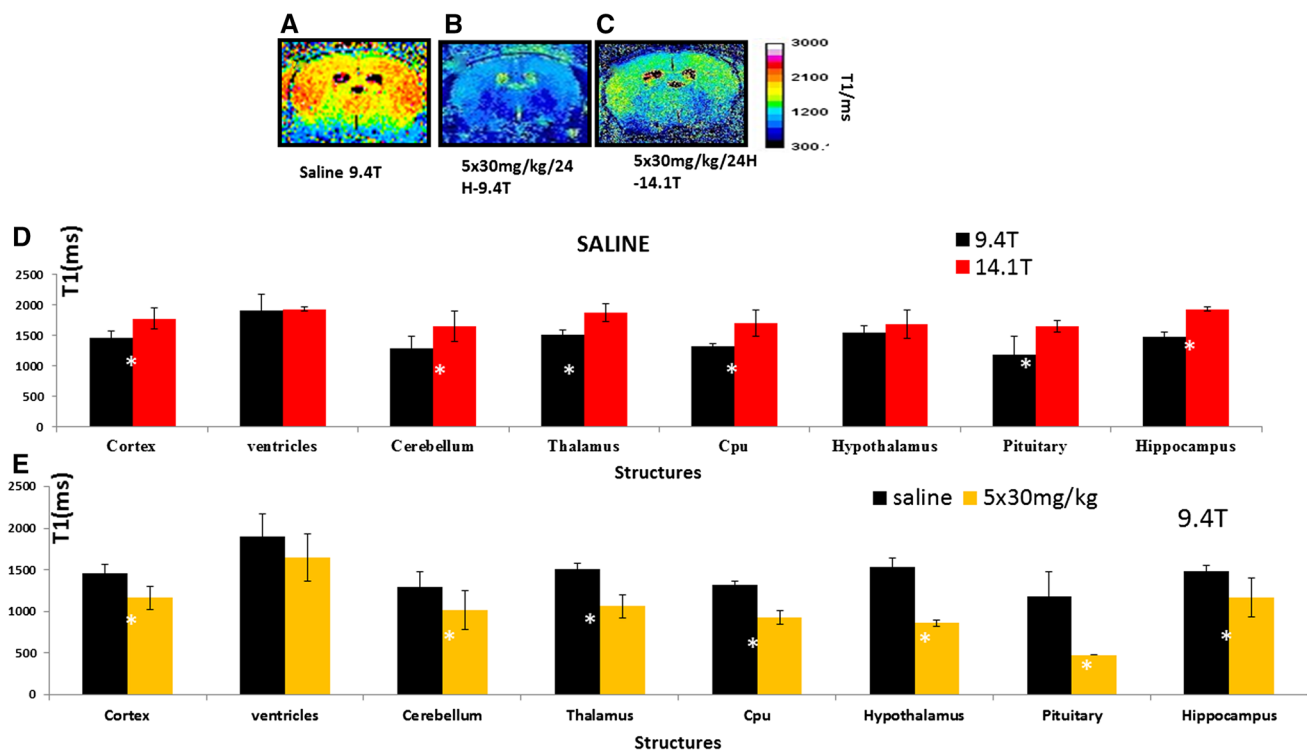


Fig. 6 T_1 mapping in mouse brain with MP2RAGE. **a** T_1 false colour-coded coronal maps in saline-injected animals and 24 h post last fractionated Mn^{2+} injection at 9.4T and 14.1T. **b** Comparison of T_1 values at 9.4T and 14.1T in different structures of the mouse brain in saline-injected animals ($n = 5$ per field strength) showing

significant increase of T_1 values at 14.1T in all the structures (* $p < 0.004$, Anova + Bonferroni). **c** A significant shortening of T_1 in Mn^{2+} -injected animals was found at 9.4T (* $p < 0.01$; ** $p < 0.0008$, Anova + Bonferroni)

their smaller brain structures require increased SNR levels. In addition, the longer T_1 values may be advantageous for discriminating between tissues [Myelin for example (Thiessen et al. 2013)]. Unfortunately, the gain in SNR expected at higher field strengths is often counteracted by uncorrected B_0 and B_1 distortions while time consuming T_1 measurements impose limited brain coverage.

At high magnetic fields ($\geq 7T$), MP2RAGE provided proton density-, T_2^* contrast- and B_1 inhomogeneity -corrected 3D T_1 -weighted images of the human brain with increased T_1 contrast. Moreover, T_1 mapping could be performed with no need for additional acquisitions providing simultaneous quantitative investigation of various interesting human brain structures (Marques and Gruetter 2013; Strotmann et al. 2014; Gizewski et al. 2014). Here the potential of MP2RAGE for imaging the mouse brain with regards to SNR, CNR and T_1 accuracy are discussed.

Efficiency of MP2RAGE for the mouse brain

In rodents, MEMRI has shown enormous potential for investigating neuronal tract tracing, neuronal activation (Auffret et al. 2016; Just and Gruetter 2011a, Just et al. 2011b) or for visualizing neuro-architecture (Bock et al.

2008; Silva et al. 2008) in combination with 3D T_1 -weighted gradient echo, inversion-recovery or spin-echo techniques (Chuang and Koretsky 2006; Allemang-Grand et al. 2015; Bertrand et al. 2013). To compensate for the low WM/GM/CSF T_1 contrast in the normal mouse brain, paramagnetic contrast with Mn^{2+} was used. To limit manganese toxicity issues, fractionated $MnCl_2$ (15 mM) intraperitoneal doses (30 mg/kg/24 h) were given across 5 days prior to the MRI sessions. No significant effects on body weight and temperature were found in accordance with previous studies (Grünecker et al. 2010; Sepúlveda et al. 2012).

As explained in the seminal paper of Marques et al. (2010), the combination of gradient echo images acquired in an interleaved manner at two different inversion times ($T_{11,2}$) with Eq. (1) reduces the SNR due to noise propagation but not necessarily the CNR as a consequence of the removal of T_2^* effects and B_1 field reception inhomogeneity. Moreover, the CNR can be optimized with regards to the desired WM/GM/CSF contrast. Here, we assumed T_1 values for WM/GM/CSF reported by (Chuang and Koretsky 2006) and Lee et al. (2005) at 11.7T with and without $MnCl_2$. We assumed a dose of 30 mg/kg of $MnCl_2$ and corresponding T_1 s although five doses at 30 mg/kg/24 h

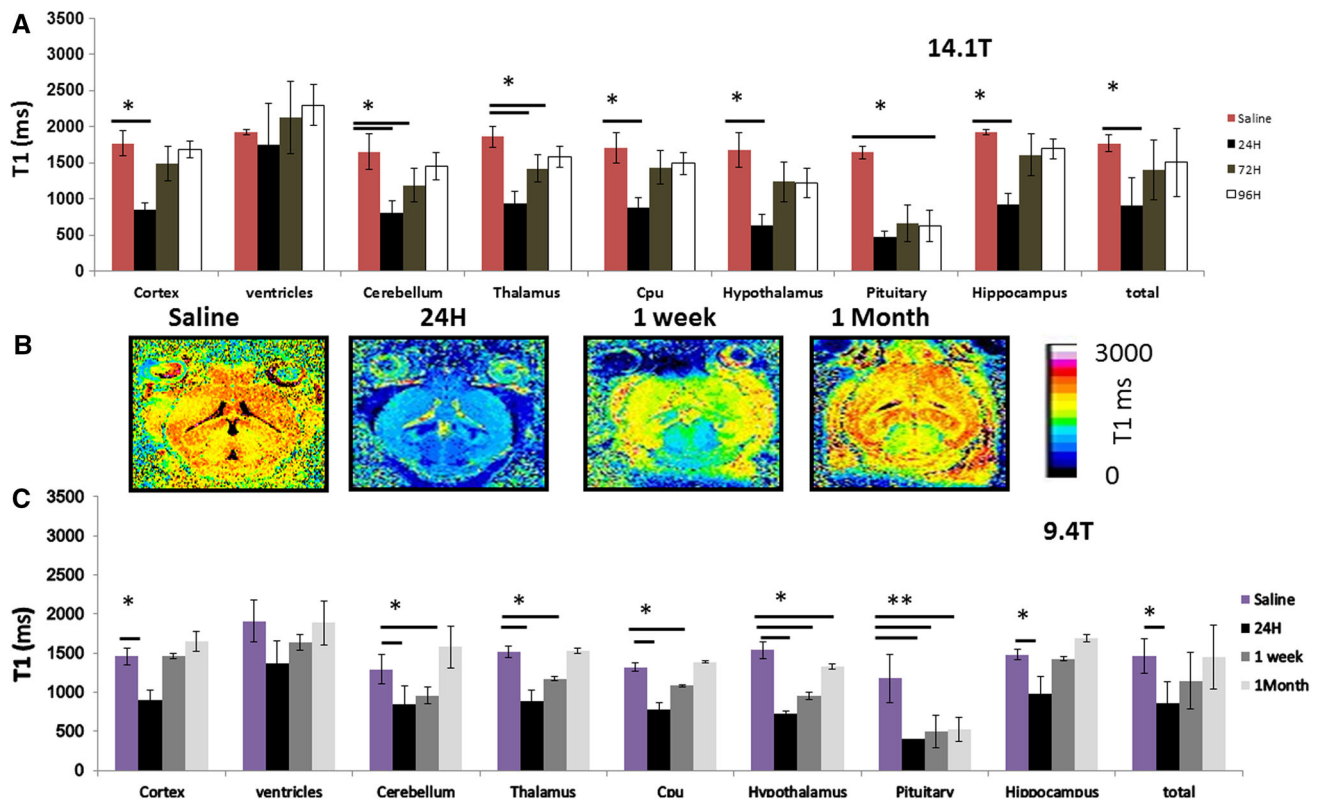


Fig. 7 T_1 mapping at 9.4T and 14.1T in the mouse brain with MP2RAGE at 24, 72, 96 h, 1 week and 1 month post- Mn^{2+} cessation **a** comparison of T_1 values at 14.1T in different regions of interest in the mouse brain up to 96 h post cessation of Mn^{2+} injection. Significant changes were found relative to saline-injected animals ($p < 0.0008$). T_1 remained significantly lower relative to T_1 values in the same ROIs in saline-injected animals 24 h post cessation of Mn^{2+} injections in all the structures. 72 h post Mn^{2+} cessation significant differences remained in the cerebellum, the thalamus and the pituitary gland in which T_1 remained significantly lower compared to saline-injected animals up to 96 h post last Mn^{2+} injection. **b** MP2RAGE horizontal T_1 maps acquired at 9.4T 24 h, 1 week and 1 month post-

cessation of fractionated Mn^{2+} injections and saline in mice and showing progressive increase of T_1 values as a function of time. **c** Comparison of T_1 values measured at 9.4T in different regions of interest in the mouse brain up to 1 month post cessation of Mn^{2+} injection showing significant differences in all ROIs 24 h after the last Mn^{2+} injection compared to saline-injected animals. 1 week post Mn^{2+} cessation, T_1 s remained significantly different from saline-injected animals in the cerebellum, hypothalamus, thalamus, caudate putamen and pituitary gland ($p < 0.05$). This last structure had still a significantly lower T_1 value compared to saline 1 month after cessation of Mn^{2+} ($p < 0.02$)

were injected. Our choice can be justified since fractionated manganese-enhanced MRI studies demonstrated that after 6×30 mg/kg IP injections in rats, T_1 values ranged between 1000 and 1500 ms in various brain structures (Bock et al. 2008) and an identical range of T_1 values was found in mice followed over 3 weeks and receiving 30 mg/kg/24 h $MnCl_2$ with a subcutaneously implanted osmotic pump (Sepúlveda et al. 2012). Moreover, Grünecker et al. (2013) relative intensity assessments after daily 30 mg/kg IP injections in mice up to 8 days also showed little changes. Simulations for $T_{11}/T_{12} = 800/2800$ ms showed that the relationship between MP2RAGE signal [Eq. (1)] and T_1 spanned the desired range between 500 and 3000 ms with an almost linear relationship for flip angles 2, 2° and 4, 4° and MP2RAGETR = 4–6 s. This “linear” range was restricted to 800–2500 ms for flip angles 7, 7°. Optimizations of CNR were based on previous simulations

using Eq. (2) performed by Marques et al. (2010). Although at different field strengths, these simulations were performed for a similar range of values to ours. Our simulations using Eq. (2) showed that CNR was enhanced for 6 s, $\alpha_1/\alpha_2 = 7/7^\circ$ and $T_{11}/T_{12} = 800\text{--}1600$ ms. In-vivo measurements corroborated these findings although noise levels remained important. In addition, our findings were in agreement with simulations and measurements performed at 7T in a human scanner showing increased CNR for an identical set of parameters (Marques and Gruetter 2013). Moreover, these measurements proved that MP2RAGE was useful for an enhanced delineation of specific grey matter structures over a restricted range of T_1 values. In mice, structures of the cerebellum were also better delineated for $T = 6$ s, $\alpha_1/\alpha_2 = 7/7^\circ$ and $T_{11}/T_{12} = 800\text{--}1600$ ms at 9.4T (Fig. 3f). However, our measurements were performed with quadrature surface coils at 9.4T and 14.1T

after FASTMAP shimming over a large voxel of interest. Although we expected a higher sensitivity with surface coils and although the shapes and transmit powers of these coils were optimized to limit B_1 transmit field inhomogeneity inherent to these coils, SA2RAGE measurements showed that B_1 transmit field distortions remained important over the lower part of the mouse brain at both fields. These effects are detrimental to the precise estimate of T_1 . In order to reduce these B_1 distortions, the pulse profiles of the MP2RAGE sequence were calibrated in $MnCl_2$ -doped phantoms. Accurate T_1 values were obtained for flip angles 2° at 9.4T and 2° , 3° at 14.1T. We used these values for further investigations in mice at both fields although they imply a CNR reduction. To tackle this issue, (Marques and Gruetter 2013) proposed a methodology using both T_1 and B_1 look-up tables and showed good results for further reducing residual transmit field distortions in MP2RAGE images. Current developments are ongoing to apply this methodology to our measurements. This is important, especially at higher field strength where distortions were more important (Fig. 2) and more difficult to correct. Besides, increased spatial resolutions are desirable but imply increasing the number of flip angles in the phase encoding direction and, therefore, increasing transmit field inhomogeneity (Marques and Gruetter 2013). Finally, although the lower SNR levels did not have a strong impact on the quality of MR images in human scanners, poor SNR levels coupled to B_1 inhomogeneity have strong effects on mouse MP2RAGE images: with an increased spatial resolution [$78 \times 78 \times 130 \mu\text{m}^3$, (Fig. 2)], noise levels were too important for clear depiction of small structures whether at 9.4T or at 14.1T. It is essential to appropriately measure noise levels to assess the quality of MR data. Here, we also used Rician distributions to calculate noise levels. We think these calculations were more appropriate than ROI estimates of standard deviations avoiding SNR and CNR overestimates (Fig. 5). Recently, solutions were provided for noise reduction in T_1 -weighted MP2RAGE images (O'Brien et al. 2014; Eggenschwiler et al. 2012) which could be easily implemented for mouse MP2RAGE. Nonetheless, the use of transmit volume coils in combination with surface receive coils should already improve the quality of MP2RAGE images, while improved hardware such as cryoprobes that become more and more available for mouse MR imaging should make the difference notwithstanding new possibilities such as parallel imaging for rodents that should at the same time decrease significantly acquisition times (Piedzia et al. 2014; Liu et al. 2011).

We were able to depict cerebellar, hippocampal, cortical, hypothalamic and olfactory bulb enhancements as in studies where $MnCl_2$ was infused through the tail vein and at higher Mn^{2+} doses (up to 175 mg/kg) (Lee et al. 2005).

Cerebellar, cortical and olfactory bulb layers were less clearly resolved as the spatial resolution was $156 \mu\text{m}^3$ isotropic instead of $100 \mu\text{m}^3$ in Lee et al. (2005). Nonetheless, small structures such as the globus pallidus (GP), inferior colliculus, anterior pretectal nucleus, anterior olfactory area and nucleus acumbens could be detected on MP2RAGE coronal images [Fig S4B-C]. All these structures are of high interest for studying subthalamic alterations in neurodegenerative studies (Callahan and Abercrombie 2015) as well as information processing and functional metabolism (Chen et al. 2015; Just et al. 2011b). The latter is interesting in the present case as specific access to targeted nuclei of the mouse brain is given using MP2RAGE measurements in combination with surface coils, thus potentially enabling MR spectroscopic studies of deep brain structures (Just et al. 2011b) as well investigations of Ca^{2+} signalling mechanisms.

T_1 mapping of the mouse brain with MP2RAGE

One of the main advantages of the MP2RAGE technique over many others is that it rapidly and easily provides high-resolution T_1 maps from T_1 -weighted and proton-density-weighted 3D GRE images. No subsequent T_1 mapping technique is needed. In the present study, two blocks of 3D MR images with a $156 \mu\text{m}$ isotropic spatial resolution were obtained in 31 min whereas conventional 3D GRE were measured in 19 min only without allowing quantitative T_1 estimates. In general, T_1 maps of the mouse brain were spatially well-resolved and allowed estimates of T_1 in different structures of the mouse brain although SNR was low. As mentioned above, the sensitivity of MP2RAGE depends on the choice of T_1 s and T_1 range. As expected, T_1 estimates in various structures of the mouse brain were significantly longer at 14.1T than at 9.4T with and without manganese-enhancement. Although further adjustments of image acquisition parameters will be necessary at 14.1T, especially for higher spatial resolutions, results were consistent with literature (van de Ven et al. 2007) and directly comparable at 9.4T. In saline-injected animals, T_1 values were only slightly shorter than those measured by Lee et al. (2005) in the same regions at 11.7T with a spin-echo inversion recovery sequence. However, T_1 values measured at 9.4T with spin-echo saturation recovery by (Sepúlveda et al. 2012) and van de Ven et al. (2007) were 1.34-fold higher. As discussed earlier, our T_1 values may have been misestimated due to our choice of parameters and hence LUT that did not include the effects of noise. We also assumed identical $T_{11,2}$ values at 9.4T and 14.1T introducing deliberately a bias at 14.1T. Improved assumptions based on in vivo measurements at this field strength will need to be performed as known values are still lacking. Previous T_1 measurements in WM and GM areas

of the rat brain obtained at 14.1T after MnCl_2 intravenous injection at a dose of 25 mg/kg were in the range 1800–2200 ms (Maddage et al. 2014) meaning that our T_1 estimates at 14.1T should probably be longer. Despite these T_1 underestimates, 24 h post-fractionated injections of MnCl_2 , T_1 values were significantly shortened in several structures compared to saline-injected mice at 9.4T and 14.1T in agreement with previous studies (Chuang and Koretsky 2006; Lee et al. 2005). Compared to T_1 values measured at 11.7T in the same structures by Lee et al. (2005), our T_1 values 24 h post- MnCl_2 were between 8 and 13 % higher at 9.4T and between 18 and 24 % higher at 14.1T except for the pituitary gland ($T_1 = 231 \pm 23.4$ ms in Lee et al.'s vs $T_1 = 478 \pm 2$ ms at 9.4T) suggesting that in our case the dose of MnCl_2 in the mouse brain was lower than 9 mg/kg. Small structures were still enhanced and detectable. Bock et al. (2008), on the other hand, measured T_1 values in rats at 7T after giving six 30 mg/kg fractionated intravenous injections of MnCl_2 . 48 h post-cessation of MnCl_2 injections, T_1 in various structures ranged between 1100 and 1500 ms. At 24 h post-cessation of MnCl_2 injections, our T_1 values ranged between 860 and 1200 ms at 9.4T in similar regions with five injections only. As described previously, our post- Mn^{2+} T_1 values may still be slightly underestimated and it would be difficult to draw conclusions given the differences between the protocols. However, the average change in T_1 between control and Mn^{2+} -injected animals yielded around 30 % in both studies.

Low Mn^{2+} doses in the mouse brain estimated with MP2RAGE T_1 mapping

To date, quantitative T_1 estimations of Mn^{2+} -enhanced structures in the mouse brain remain sparse and comparative studies remain difficult due to differing protocols (doses, injection routes, field strength...) as well as time-consuming T_1 mapping techniques. As manganese becomes an interesting compound for cancer research (Patrick et al. 2015), studies on T_1 relaxivity for estimating Mn^{2+} concentrations are of paramount importance in addition to the possibility of performing translational clinical studies for which neurotoxicity of manganese needs to be minimal (Botsikas et al. 2012). Moreover, identification of Mn^{2+} concentrations could serve as a means to follow Ca^{2+} pathways and rates during brain activation (Sepúlveda et al. 2012), while the possibility to measure low Mn^{2+} concentrations could help differentiating cell densities as well as release/uptake rates (Chuang and Koretsky 2006). We examined the effects of Mn^{2+} clearance on the T_1 of several brain structures of the mouse brain. 1 month after cessation of manganese, almost all the

mouse brain structures had recovered to the T_1 levels of saline-injected mice except for the pituitary gland for which T_1 values were not significantly different from T_1 1 week and 24 h-post cessation of manganese. Our results confirm previous findings (Grünecker et al. 2013; Sepúlveda et al. 2012). Grünecker et al. (2013) investigated regional accumulation and clearance in the mouse brain using fractionated manganese injections using semi-quantitative methods. Their study showed that clearance of Mn^{2+} happened between 5 and 7 days (half-lives) in significant contrast to previous studies in other species. However, T_1 mapping techniques show increased robustness and stronger potential for differentiating smaller regions of interest. For example, (Sepúlveda et al. 2012) were able to estimate T_1 differences between structures of the cerebellum and of the hippocampus during Mn^{2+} accumulation and during clearance. A priori, infusion of Mn^{2+} through mini-osmotic pumps at a dose of 30 mg/kg and fractionated injections at the same dose appear to lead to similar regional T_1 values. Further, (Chuang and Koretsky 2006) showed that the pituitary gland T_1 decreased significantly at a dose of 9 mg/kg MnCl_2 but decreased much more slowly at high doses up to 175 mg/kg. This was attributed to a limited ability of the pituitary gland to transport Mn^{2+} . Patients affected with manganese encephalopathy presented high T_1 -weighted signal intensities of the pituitary gland (Dolgan et al. 2015) while other studies demonstrated that pituitary hormone secretion was modified in Parkinsonian patients (Schaefer et al. 2008). Thus, investigations of the pituitary gland in rats and mice with MP2RAGE upon chronic exposure to manganese could be of particular interest as manganese causes neurological effects similar to Parkinson's disease and could give new insights into the underlying mechanisms of this neurodegenerative disease (Sepúlveda et al. 2012).

Conclusion

Previous studies at high field in humans showed the huge potential of MP2RAGE for structural MR imaging. Although adjustments in terms of SNR and CNR will be necessary for further use at high fields in rodents, we demonstrated that MP2RAGE can be an interesting quantitative technique in combination with Manganese-Enhanced Magnetic Resonance Imaging. MP2RAGE T_1 mapping represents an interesting tool for further investigation of transgenic mouse models and, therefore, an interesting instrument for further translational studies. Future studies with MP2RAGE in mice will focus on CNR optimization, noise reduction and improvements of the spatial resolution.

Acknowledgments This work was supported by the Centre d'Imagerie Biomédicale (CIBM) and Ecole Polytechnique Fédérale de Lausanne (EPFL). We would like to thank Professor Rolf Gruetter for contributing to the animals, materials and analysis tools, Dr Olivier Reynaud for programming the reconstruction macros and Dr José Marques for the few useful discussions and for sharing his programming tools.

Compliance with ethical standards

Conflict of interest The authors declare no conflict of interest.

References

- Allemand-Grand R, Scholz J, Ellegood J, Cahill LS, Laliberté C, Fraser PE, Josselyn SA, Sled JG, Lerch JP (2015) Altered brain development in an early-onset murine model of Alzheimer's disease. *Neurobiol Aging* 36(2):638–647. doi:10.1016/j.neurobiolaging.2014.08.032
- Auffret M, Samim I, Lepore M, Gruetter R, Just N (2014) Quantitative activity-induced manganese-dependent MRI for characterizing cortical layers in the primary somatosensory cortex of the rat. *Brain Struct Funct* 221(2):695–707
- Bertrand A, Khan U, Hoang DM, Novikov DS, Krishnamurthy P, Rajamohamed Sait HB, Little BW, Sigurdsson EM, Wadghiri YZ (2013) Non-invasive, in vivo monitoring of neuronal transport impairment in a mouse model of tauopathy using MEMRI. *Neuroimage* 64:693–702. doi:10.1016/j.neuroimage.2012.08.065
- Bock NA, Paiva FF, Silva AC (2008) Fractionated manganese-enhanced MRI. *NMR Biomed* 21(5):473–478
- Botsikas D, Terraz S, Vinet L, Lamprianou S, Becker CD, Bosco D, Meda P, Montet X (2012) Pancreatic magnetic resonance imaging after manganese injection distinguishes type 2 diabetic and normoglycemic patients. *Islets* 4(3):243–248. doi:10.4161/isl.20857
- Callahan JW, Abercrombie ED (2015) Age-dependent alterations in the cortical entrainment of subthalamic nucleus neurons in the YAC128 mouse model of Huntington's disease. *Neurobiol Dis* 78:88–99. doi:10.1016/j.nbd.2015.03.006
- Canals S, Beyerlein M, Keller AL, Murayama Y, Logothetis NK (2008) Magnetic resonance imaging of cortical connectivity in vivo. *Neuroimage* 40(2):458–472. doi:10.1016/j.neuroimage.2007.12.007
- Chen MC, Ferrari L, Sacchet MD, Foland-Ross LC, Qiu MH, Gotlib IH, Fuller PM, Arrigoni E, Lu J (2015) Identification of a direct GABAergic pallidocortical pathway in rodents. *Eur J Neurosci* 41(6):748–759. doi:10.1111/ejn.12822
- Cheng T, Magill AW, Comment A, Lei H (2014) Ultra-high field birdcage coils: a comparison study at 14.1T. *Conf Proc IEEE Eng Med Biol Soc* 2014:2360–2363. doi:10.1109/EMBC.2014.6944095
- Chuang KH, Koretsky A (2006) Improved neuronal tract tracing using manganese enhanced magnetic resonance imaging with fast T(1) mapping. *Magn Reson Med* 55(3):604–611
- Dolgan A, Budrewicz S, Koszewicz M, Bładowska J, Slotwinski K, Zagrajek M, Koziorowska-Gawron E, Podemski R (2015) Acute hyperkinetic syndrome due to ephedrone abuse. *J Addict Med* 9(3):244–245. doi:10.1097/ADM.0000000000000048
- Eggenschwiler F, Kober T, Magill AW, Gruetter R (2012) Marques JP.SA2RAGE: a new sequence for fast B1 + -mapping. *Magn Reson Med* 67(6):1609–1619. doi:10.1002/mrm.23145
- Gizewski ER, Maderwald S, Linn J, Dassinger B, Bochmann K, Forsting M, Ladd ME (2014) High-resolution anatomy of the human brain stem using 7-T MRI: improved detection of inner structures and nerves? *Neuroradiology* 56(3):177–186. doi:10.1007/s00234-013-1312-0
- Grünecker B, Kaltwasser SF, Zappe AC, Bedenk BT, Bicker Y, Spoomaker VI, Wotjak CT, Czisch M (2013) Regional specificity of manganese accumulation and clearance in the mouse brain: implications for manganese-enhanced MRI. *NMR Biomed* 26:542–556
- Grünecker B, Kaltwasser SF, Peterse Y, Zappe AC, Bedenk BT, Bicker Y, Spoomaker VI, Wotjak CT, Czisch M (2010) Fractionated manganese injections: effects on MRI contrast enhancement and physiological measures in C57BL/6 mice. *NMR Biomed* 23(8):913–921. doi:10.1002/nbm.1508
- Just N, Gruetter R (2011) Detection of neuronal activity and metabolism in a model of dehydration-induced anorexia in rats at 14.1 T using manganese-enhanced MRI and 1H MRS. *NMR Biomed* 24(10):1326–1336. doi:10.1002/nbm.1694
- Just N, Cudalbu C, Lei H, Gruetter R (2011) Effect of manganese chloride on the neurochemical profile of the rat hypothalamus. *J Cereb Blood Flow Metab* 31(12):2324–2333. doi:10.1038/jcbfm.2011.92
- Kober T, Granziera C, Ribes D, Browaeys P, Schlupe M, Meuli R, Frackowiak R, Gruetter R, Krueger G (2012) MP2RAGE multiple sclerosis magnetic resonance imaging at 3 T. *Invest Radiol* 47(6):346–352. doi:10.1097/RLI.0b013e31824600e9
- Labadie C, Lee JH, Rooney WD, Jarchow S, Aubert-Frécon M, Springer CS Jr, Möller HE (2014) Myelin water mapping by spatially regularized longitudinal relaxographic imaging at high magnetic fields. *Magn Reson Med* 71(1):375–387. doi:10.1002/mrm.24670
- Lee JH, Silva AC, Merkle H, Koretsky AP (2005) Manganese-enhanced magnetic resonance imaging of mouse brain after systemic administration of MnCl₂: dose-dependent and temporal evolution of T1 contrast. *Magn Reson Med* 53(3):640–648
- Liu JV, Bock NA, Silva AC (2011) Rapid high-resolution three-dimensional mapping of T1 and age-dependent variations in the non-human primate brain using magnetization-prepared rapid gradient-echo (MPRAGE) sequence. *Neuroimage* 56(3):1154–1163. doi:10.1016/j.neuroimage.2011.02.075
- Maddage R, Marques J, Gruetter R (2014) Phase-based manganese-enhanced MRI, a new methodology to enhance brain cyto architectural contrast and study manganese uptake. *Magn Reson Med* 72:1246–1256
- Marques JP, Gruetter R (2013) New developments and applications of the MP2RAGE sequence—focusing the contrast and high spatial resolution R1 mapping. *PLoS One* 8(7):e69294. doi:10.1371/journal.pone.0069294
- Marques JP, Kober T, Krueger G, van der Zwaag W, Van de Moortele PF, Gruetter R (2010) MP2RAGE, a self bias-field corrected sequence for improved segmentation and T1-mapping at high field. *Neuroimage* 49(2):1271–1281. doi:10.1016/j.neuroimage.2009.10.002
- O'Brien KR, Kober T, Hagmann P, Maeder P, Marques J, Lazeyras F, Krueger G, Roche A (2014) Robust T1-weighted structural brain imaging and morphometry at 7T using MP2RAGE. *PLoS One* 9(6):e99676. doi:10.1371/journal.pone.0099676
- Patrick PS, Rodrigues TB, Kettunen MI, Lyons SK, Neves AA, Brindle KM (2015) Development of Timd2 as a reporter gene for MRI. *Magn Reson Med*. doi:10.1002/mrm.25750
- Paxinos G, Watson C (1998) The rat stereotaxic coordinates. Academic Press, San Diego
- Piędzia W, Jasiński K, Kalita K, Tomanek B, Węglarz WP (2014) White and gray matter contrast enhancement in MR images of the mouse brain in vivo using IR UTE with a cryo-coil at 9.4 T.

- J Neurosci Methods 30(232):30–35. doi:[10.1016/j.jneumeth.2014.04.019](https://doi.org/10.1016/j.jneumeth.2014.04.019)
- Rajan J, Poot D, Juntu J, Sijbers J (2010) Noise measurement from magnitude MRI using local estimates of variance and skewness. *Phys Med Biol* 55:N441–N449
- Schaefer S, Vogt T, Nowak T, Kann PH, German KIMS board (2008) Pituitary function and the somatotrophic system in patients with idiopathic Parkinson's disease under chronic dopaminergic therapy. *J Neuroendocrinol* 20(1):104–109
- Sepúlveda MR, Dresselaers T, Vangheluwe P, Everaerts W, Himmelreich U, Mata AM, Wuytack F (2012) Evaluation of manganese uptake and toxicity in mouse brain during continuous MnCl₂ administration using osmotic pumps. *Contrast Media Mol Imaging* 7(4):426–434. doi:[10.1002/cmml.1469](https://doi.org/10.1002/cmml.1469)
- Silva AC, Lee JH, Aoki I, Koretsky AP (2004) Manganese-enhanced magnetic resonance imaging (MEMRI): methodological and practical considerations. *NMR Biomed* 17:532–543
- Silva AC, Lee JH, Wu CW, Tucciarone J, Pelled G, Aoki I, Koretsky AP (2008) Detection of cortical laminar architecture using manganese-enhanced MRI. *J Neurosci Methods* 167(2):246–257
- Strotmann B, Heidemann RM, Anwander A, Weiss M, Trampel R, Villringer A, Turner R (2014) High-resolution MRI and diffusion-weighted imaging of the human habenula at 7 tesla. *J Magn Reson Imaging* 39(4):1018–1026. doi:[10.1002/jmri.24252](https://doi.org/10.1002/jmri.24252)
- Thiessen JD, Zhang Y, Zhang H, Wang L, Buist R, Del Bigio MR, Kong J, Li XM, Martin M (2013) Quantitative MRI and ultrastructural examination of the cuprizone mouse model of demyelination. *NMR Biomed* 26(11):1562–1581. doi:[10.1002/nbm.2992](https://doi.org/10.1002/nbm.2992)
- Tkác I, Henry PG, Andersen P, Keene CD, Low WC, Gruetter R (2004) Highly resolved in vivo ¹H NMR spectroscopy of the mouse brain at 9.4 T. *Magn Reson Med* 52(3):478–484
- van de Ven RC, Hogers B, van den Maagdenberg AM, de Groot HJ, Ferrari MD, Frants RR, Poelmann RE, van der Weerd L, Kiihne SR (2007) T(1) relaxation in in vivo mouse brain at ultra-high field. *Magn Reson Med* 58(2):390–395